Invited Paper

FoMR
Frontiers of Multidisciplinary Research

Interstitial Fluid Pressures Generated during Negative Pressure Therapy (NPT) On Intact Skin: A Poro-Hyperelastic Modeling Study

Kris Kieswetter[a], *Balakrishna Haridas[b]

ABSTRACT

Negative Pressure Therapy (NPT) has emerged recently as a potential option for controlled, precise management of post operative swelling in and around closed surgical incisions in the pursuit of reducing surgical complications. This study examines the underlying mechanism of action (MOA) involved during application of NPT to intact skin/closed incisions and specifically evaluates the effects of NPT on interstitial fluid flow and transport using a finite element model. A two-dimensional (2D) plane-strain poro-hyperelastic finite element analysis (FEA) model of a distal femoral/thigh limb cross section was developed to analyze the interstitial fluid pressure fields generated in the underlying epidermis, dermis, subcutaneous fat, and muscle during NPT application for various pressure levels and dressing configurations. Results demonstrate a dose-dependent response relationship between the device parameters (negative pressure (NP) level, dressing contact angle) and negative interstitial fluid pressures (hydrostatic tension values) in soft tissue layers beneath the dressing contact zone. These tissue distensions are likely to actuate lymphatic pores (initial lymphatics) and lymphatic capillaries, enhancing fluid clearance without drain collection, potentially reducing post-operative edema around the incision site and surrounding tissue envelope. Reducing edema risks following a surgical procedure may help facilitate early ambulation and patient compliance with post-operative rehabilitation protocols, potentially assisting with the restoration of muscle strength and range of motion, thereby helping improve the prognosis for improved long-term recovery.

Received date: 15.09.2025
Accepted date: 30.11.2025

Keywords: Negative Pressure Therapy, Intact Skin, Seroma, Edema, Poro-Hyperelasticity, Finite Element Analysis, Interstitial Fluid Pressure, Lymphatics

https://doi.org/10.65601/FoMR.2026.1.1.1

[a]*Global R&D Director, Medical Surgical Business*
Solventum Inc.
6203 Farinon Road, San Antonio, TX 78249.
kmkieswetter@solventum.com

***Corresponding Author:**
[b]*Device & Implant Innovations LLC*
1008 Muirfield Vlg, College Station, TX 77845
bharidas@diinnovations.com
Professor-of-Practice, Department of Biomedical Engineering
Deputy Executive Director, FDA Southwest Pediatric Devices Innovation Consortium (www.swpdc.org) Texas A&M University
101 Bizzell St., 3120 TAMU, College Station, TX 77843
bharidas@tamu.edu

INTRODUCTION

Surgical site swelling, seromas and hematomas increase post-operative pain and risk of infections and are amongst the most frequent complications seen in patients undergoing total knee arthroplasty (*TKA*) and other procedures involving substantial soft tissue dissection & manipulation (Holm et al., 2010; Szöts et al., 2015). The interstitial fluid buildup in and around these surgically created wounds are known to be the most likely cause of edema and related post-surgical complications which originate because of impaired lymphatic systems coupled with inflammatory conditions. These complications include delayed wound healing, suboptimal physiotherapy outcomes & return to ambulation, and overall increase in post-operative recovery time.

A range of treatment options have been explored for management of post-surgical swelling and seromas in TKA. These include cold compression, elastic bandaging, compression bandages and compression therapy (Brock et al., 2017; Munk et al., 2013) which rely on applying compression to the limb or tissue to reduce the retention of fluid in the tissue compartments. The primary mechanism in these treatments is believed to be that of generating a hydrostatic compressive stress/fluid over-pressure in the soft tissue that impedes fluid egress from the capillary bed into tissue, as well as enhancing fluid transport into the lymphatics. The efficacy of compression therapy for TKA is not yet well understood due to lack of controlled studies reported in clinical literature and heterogenous approaches across studies (Brock et al., 2017). It is also challenging to quantify compression levels in many of these passive devices (e.g., bandages) since the input parameter, i.e., compressive stress or pressure is not directly measured or precisely controlled in these studies, further making it challenging to draw clear conclusions on efficacy and outcomes.

Negative Pressure Therapy (NPT) has emerged recently as a potential option for controlled and precise management of post operative swelling in and around closed surgical incisions. In recent clinical studies and case series, NPT applied to closed surgical incisions on high energy trauma and open fracture sites has lowered wound dehiscence and infection rates (Stannard et al., 2009; Stannard et al., 2006; Stannard et al., 2009) indicating the potential of this therapeutic approach for reducing complications. Other clinical studies (Pachowsky et al., 2012; Pauser et al., 2014) also indicate that NPT applied to closed surgical incision sites and/or over intact skin following surgical interventions for femoral neck fracture and total knee replacements likely reduce the incidence of seroma and hematoma formation (Figure 1). Well controlled preclinical studies in a porcine model **(Kilpadi & Cunningham 2011),** with NPT applied to closed surgical incisions showed statistically significant (63%) reductions in hematomas and seromas. This study Kilpadi & Cunningham (2011) demonstrated increased lymphatic clearance as tracked via enhanced transport of radiolabeled nanoparticle tracers to lymph nodes, concomitant with reduced fluid collection in the wound canister. Clearly, there is a need to further elucidate the underlying mechanism of action (MOA) involved during application of NPT

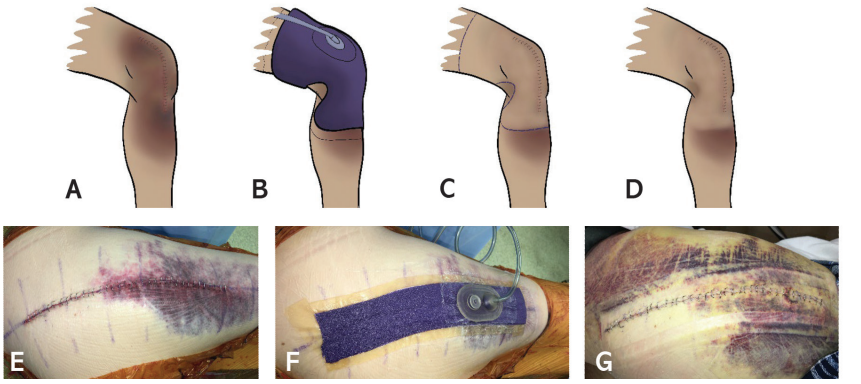

Figure 1 Representative images of TKA, prior to (A), with application of (B), and following removal of (C, D) of ciNPT dressing that covers the incision, a broad tissue envelope and a wide wrap angle (outlined in C). Intra-operative images prior to (E) and following (F) application of ciNPT dressing over incision. Dressing removal at post-operative day 8 (G) showed improved hematoma resolution relative to adjacent untreated areas. A similar image has been reported by Pauser et al. (2014). Clinical images courtesy of Animesh Agarwal, MD.

to intact skin/closed incisions to understand the role of the therapy in interstitial fluid flow and transport.

The evidence seen in these prior clinical and preclinical studies raises some interesting questions related to the interplay between the application of NPT at the skin surface, and the resulting biomechanical effects in the soft tissue layers beneath the surface of skin. Specifically, it would be of interest to understand the biomechanical interactions between NPT applied to the skin surface (Figure 2) and the resulting deformations in the surface and deep tissue layers that in turn, alter the interstitial fluid pressures and flow/transport.

Figure 2 3M™ Prevena Restor™ Incision Management System applied to a closed incision in a TKA patient.

Interstitial fluid pressures are generated due to the well-known phenomenon of **poro-hyperelasticity** or biphasic behavior of soft hydrated tissues (Barsimantov et al. 2024, Xu et al., 2024; Lavigne et al., 2025; Fahlgren et al., 2012; Oomens et al., 1987) wherein mechanical loads produce tissue deformations which in turn, induce elevations or reductions in the interstitial fluid pressures (pore pressures). *Poro-hyperelasticity in this context specifically refers to the mechanism of coupling between solid phase deformation (modeled as a hyperelastic solid) and fluid pressurization and pressure gradients which result in transport/flow of the fluid phase via diffusion through the solid matrix (modeled as a porous material with interstitial fluid flow).* When these coupled biomechanical effects are produced, i.e., tissue deformation and interstitial fluid pressure and flow, they are likely to induce corresponding changes in the biomechanics of the initial lymphatic vessels, and distension/contraction of the draining lymphatic channels. This hierarchical coupling between macro-level tissue mechanics and the likely micro-level engagement of fluid flow into and within the lymphatics potentially influence the clearance of serosanguinous infiltrate introduced interstitially due to inflammation and elevated capillary permeability. Based on these prior clinical and preclinical observations of studies on foam-based ***closed incision Negative Pressure Therapy*** **(ciNPT)** (Pachowsky et al., 2012; Pauser et al., 2014; Kilpadi & Cunningham, 2011) and current computational and finite element analysis tools available to model tissue poro-hyperelasticity (Barsimantov et al. 2024, Xu et al., 2024; Lavigne et al., 2025; Dassault Systèmes Simulia Corp., 2017; Fahlgren et al., 2012; Hendriks, 2005; Livarinen et al., 2016; Oomens et al., 1987; Wheatley et al., 2017), it is possible to quantify the variation in interstitial fluid pressure fields. Such an understanding and quantification of the interstitial pressure distributions will enable further elucidation of the potential mechanisms of action involved during NPT application to soft tissue and help design more focused preclinical or clinical studies to study the mechanism of action of NPT and lymphatic clearance.

This study describes the development of a poro-hyperelastic finite element model of a distal femoral/thigh limb cross section to explore the following key research questions related to the MOA of NPT applied to intact skin.

1. What are the potential effects of NP level (0 to -125 mmHg) on spatial variations in interstitial

fluid pressure fields in tissue layers (dermis, fat, and muscle) beneath intact skin?

2. What are the effects of the circumferential wrap angle of a foam based ciNPT dressing on the spatial variations in interstitial fluid pressures in tissue layers during NPT application?

MATERIALS & METHODS

Two-dimensional (2D) plane-strain poro-hyperelastic finite element analysis (FEA) models were developed to analyze the biomechanical response during application of NP via a foam-based ciNPT system to intact tissue. The model simulates the nonlinear mechanics of an NPT dressing and drape applied to a femoral cross section proximal to the knee (mid-thigh) containing the epidermis, dermis, subcutaneous fat, muscle, and bone regions (Fig 3). The resulting model is utilized to examine the dose response relationships between NP level and dressing wrap angle on the variations in interstitial fluid pressure distributions in the soft tissue layers below the dressing.

Geometric Abstraction

The anatomical portion of the model was derived from a publicly available online site (*https://radiopaedia.org/cases/normal-mri-of-the-thigh?lang=us; image dataset first downloaded on September 15, 2018*). This image contained cross sectional magnetic resonance imaging (MRI) data for the left mid-thigh (Figure 3) region proximal to the patella, representing approximately the proximal femoral segment of a surgical incision created for a TKA procedure. The tissue layers in the limb cross section were segmented into the epidermis, dermis, fat, muscle and bone compartments to allow for representation of a heterogenous set of hyperelastic (epidermis) and poro-hyperelastic (dermis, fat, muscle) soft tissue properties (Figure 3). The major muscles in the thigh were all combined into one single compartment to decrease computational complexity (Figure 3).

FEA Modeling of Tissue Layers

The resulting segmented geometric model was converted into an FEA model in the ABAQUS™ Software (Dassault Systèmes Simulia Corp.,2017). The dermis, fat, and muscle were modeled in ABAQUS™ (Figure 4) using plane strain poro-hyperelastic elements – CPE4P (Dassault Systèmes Simulia Corp., 2017). The constitutive response was modeled using experimental data from prior studies (Fahlgren et al., 2012; Oomens et al., 1987; Wheatley et al., 2017; Oomens et al., 2001; Wilkes et

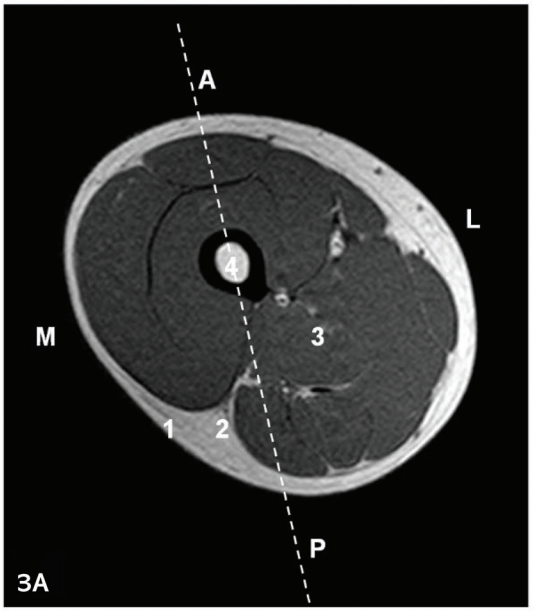

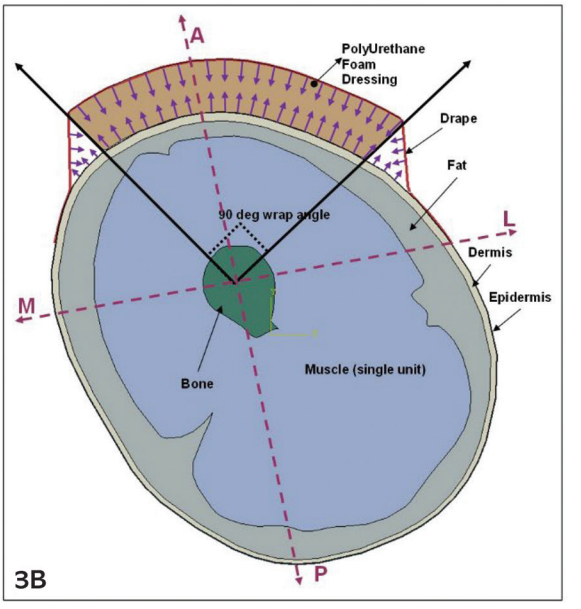

Figure 3 (A,B) Normal compartmental anatomy of the left mid-thigh cross section with major layers denoted as follows: 1 – Epidermis, dermis, 2- Fat, 3 – Muscles of the Thigh, 4 – Shaft of Femur (Bone) & Bone Marrow. Letters A, M, L, P indicate anterior, medial, lateral, and posterior locations. (B) Segmented regions of the thigh cross section, as well as layout of an NPT dressing and drape in the 90-degree wrap angle configuration.

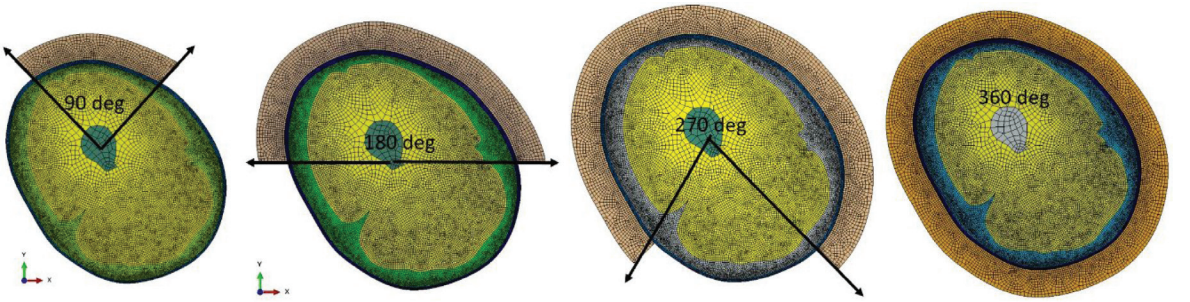

Figure 4 Finite element analysis model and meshes for the 4 different NPT dressing wrap angles (90, 180, 270, and 360 degrees)

al., 2012. Briefly, these models included Polynomial or Ogden hyperelastic strain energy functions with associated material constants for the solid phase (Table 1), and fluid permeability constant(s) (*k* – Table 1) to describes the fluid flow through the porous solid skeleton in response to deformation induced changes in interstitial fluid (pore) pressure (Dassault Systèmes Simulia Corp., 2017; Fahlgren et al., 2012; Oomens et al., 1987; Wheatley et al., 2017; Oomens et al., 2001; Wilkes et al., 2012). The epidermis and dermis were represented with plane strain elements (Figure 4) and modeled as an impermeable hyperelastic material represented using a Polynomial hyperelastic strain energy function, while bone was modeled using a linear elastic constitutive model (Table 1). Based on the orders of magnitude differences between bone and soft tissue mechanical properties, the bony region of this model was expected to behave as a rigid body. In addition to the solid phase constitutive properties, fluid permeability constants, *k*, were specified for the dermis, fat, and muscle to enable the simulation of coupled tissue deformation, interstitial fluid pressure and flow (Table 1) (Fahlgren et al., 2012; Oomens et al., 1987; Wheatley et al., 2017; Oomens et al., 2001; Wilkes et al., 2012).

FEA Modeling of the Dressing

FEA models of the NPT dressing and drape geometries placed over intact skin on the thigh with four different dressing wrap angles (90, 180, 270 and 360 degrees) were developed (Figure 4). A currently used ciNPT dressing (*3M™ Prevena Restor™ Incision Management System, 3M, Inc., Saint Paul, MN, USA*) was incorporated in this model in contact with the skin to simulate application of NPT. The NPT foam dressing portion of the model was modeled using plane strain elements with material behavior represented using the *Hyperfoam* constitutive model in ABAQUS™ (Table 1). The drape was modeled with one dimensional beam elements representing the tensile and bending stiffness of the drape material, with the material response represented using the Ogden hyperelastic constitutive model. Material constants for all the dressing components and the tissue layers were extracted from prior work (Dassault Systèmes Simulia Corp., 2017; Fahlgren et al., 2012; Oomens et al., 1987; Wheatley et al., 2017; Oomens et al., 2002; Wilkes et al., 2012) and are summarized in Table 1.

Coordinate Systems & Dressing Wrap Angle

Coordinate axes were defined and centered at the intersection of the anterior-poster plane and medial-lateral plane within the marrow cavity space [Figures 3, 4]. The dressing wrap angle was defined as the angle created by the intersection of the lines extending parallel to the edges of the foam portion of the dressing through the origin of the coordinate system [Figures 3,4]. Frictional interaction between dressing and skin was modeled to mimic perfect stick (no slip) conditions as well as a Coulomb friction coefficient of 0.25 to examine the effect of interface friction on the output variables.

Loading & Boundary Conditions

NP was applied to the exposed surfaces of the dressing, drape and tissue as a linear ramp from 0 to –125 mmHg, i.e., 0 to -0.0167 MPa (Figure 4). This ramp occurred over a 90-second time frame corresponding to clinically relevant dressing use protocols. The inner surface of the bone was fixed in the *x* and *y* directions to constrain the model and prevent rigid body translational modes. The resulting FEA models were run in the time domain using the

Table 1 Material Types, Hyperelastic Models, Permeability Models and associated constants utilized in FEA model

Material Type *(Tissue or Dressing)*	**Mechanical Model**	**Solid Phase Strain Energy (SE) Function** [Source]	**SE Functions (*W*) & Material Constants** *(SI units)*	**Fluid Permeability Constant - *k*** *(mm^4/N-s)* [Source]
Epidermis *(Tissue)*	Hyperelastic Solid	Polynomial [Stannard et. al., 2009]	$U = \sum_{i+j=1}^{N} C_{ij}(\bar{I}_1 - 3)^i(\bar{I}_2 - 3)^j + \sum_{i=1}^{N} \frac{1}{Di}(J_{el} - 1)^{2i}$; For N=2 C_{10} = 0.0094 N/mm^2; C_{01} = 0.0; C_{11} = 0.0820 N/mm^2; D_1 = 0.25 mm^2/N; D_2 = 0.0	N/A
Dermis *(Tissue)*	Poro-Hyperelastic	Polynomial [Stannard et. al., 2009]	$U = \sum_{i+j=1}^{N} C_{ij}(\bar{I}_1 - 3)^i(\bar{I}_2 - 3)^j + \sum_{i=1}^{N} \frac{1}{Di}(J_{el} - 1)^{2i}$; For N=2 C_{10} = 0.0094 N/mm^2; C_{11} = 0.0820 N/mm^2 C_{01} = 0.0; D_1 = 0.25 mm^2/N; D_2 = 0.0	0.0035 [Fahlgren et. al., 2012]
Fat *(Tissue-Adipose)*	Poro-Hyperelastic	Ogden [Kilpadi et. al., 2011]	$U = \sum_{i=1}^{N} \frac{2\mu}{\alpha^2}[\bar{\lambda}_1^{\alpha_i} + \bar{\lambda}_2^{\alpha_i} + \bar{\lambda}_3^{\alpha_i} - 3\ ] + \sum_{i=1}^{N} \frac{1}{Di}(J_{el} - 1)^{2i}$; For N=1 μ_1= 0.05 N/mm^2; α_1 = 5.0 ; D_1 = 1.0 N/mm^2	16.00 [Fahlgren et. al., 2012]
Muscle *(Tissue)*	Poro-Hyperelastic	Ogden [Kilpadi et. al., 2011]	$U = \sum_{i=1}^{N} \frac{2\mu}{\alpha^2}[\bar{\lambda}_1^{\alpha_i} + \bar{\lambda}_2^{\alpha_i} + \bar{\lambda}_3^{\alpha_i} - 3\ ] + \sum_{i=1}^{N} \frac{1}{Di}(J_{el} - 1)^{2i}$; For N=1 μ_1= 0.18 N/mm^2 ; α_1 = 30.0 ; D_1=0.25 mm^2/N	74.00 [Fahlgren et. al., 2012]
Bone *(Tissue)*	Linear Elastic	Linear Elastic [14]	E = 10,000.00 N/mm^2 ; ν = 0.3	
Drape *(Dressing)*	Hyperelastic Solid	Ogden [Wilkes et. al., 2012]	$U = \sum_{i=1}^{N} \frac{2\mu}{\alpha^2}[\bar{\lambda}_1^{\alpha_i} + \bar{\lambda}_2^{\alpha_i} + \bar{\lambda}_3^{\alpha_i} - 3\ ] + \sum_{i=1}^{N} \frac{1}{Di}(J_{el} - 1)^{2i}$; For N=2 μ_1= 0.0147 N/mm^2 ; α_1 = 4.3; μ_2= 5.440 N/mm^2; α_2 = -1.97; D_1 = 0.01 mm^2/N D_2 = 0.0 mm^2/N	N/A
Foam *(Dressing)*	Hyperfoam Solid	Hyperfoam Hill [Wilkes et. al., 2012]	$U = \sum_{i=1}^{N} \frac{2\mu}{\alpha^2}[\bar{\lambda}_1^{\alpha_i} + \bar{\lambda}_2^{\alpha_i} + \bar{\lambda}_3^{\alpha_i} - 3\ ] + \sum_{i=1}^{N} \frac{1}{\beta i}\left(J_{el}^{-\alpha_i\beta_i} - 1\right)$; For N=2 μ_1= 0.0255 N/mm^2; α_1 = 25.0 μ_2= 1.22 × 10^{-5} N/mm^2 ; α_2 = -2.15 ν_1 = 0.0; ν_2 = 0.0	N/A

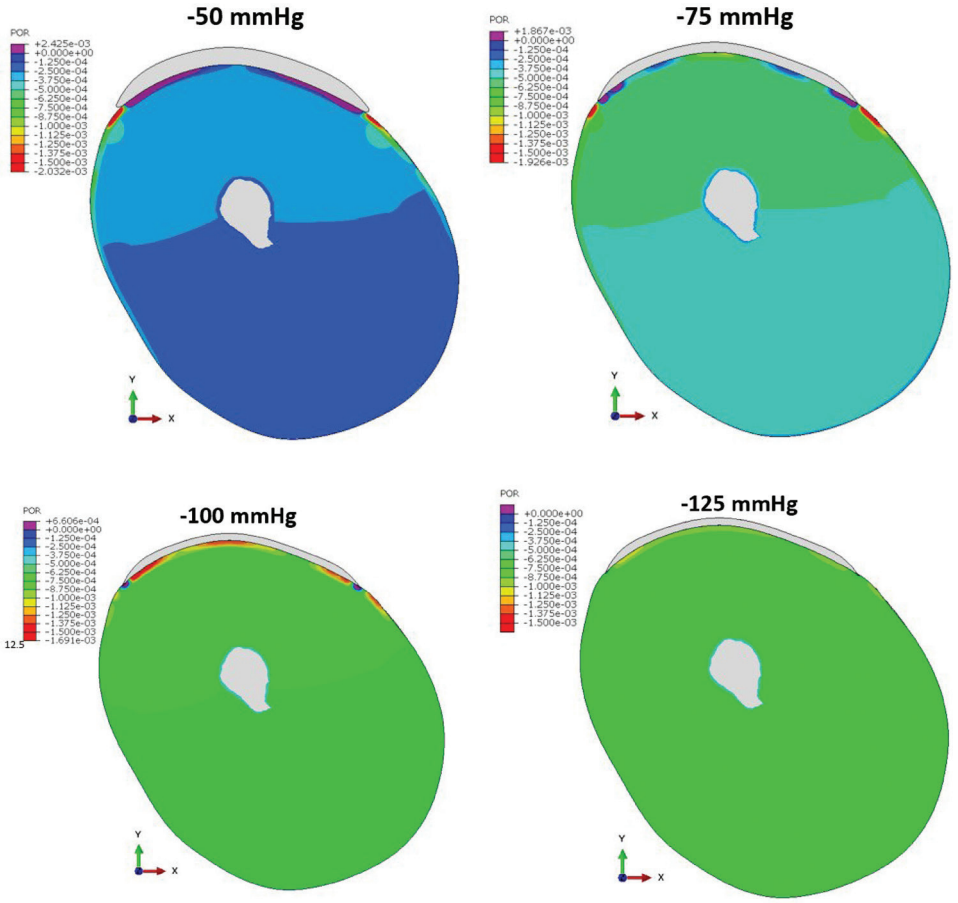

Figure 5 Dressing deformations (collapse) and interstitial fluid (pore) pressure contours as a function of increasing negative pressure (-50, -75, -100, -125 mmHg) at the 90-degree wrap angle. Negative pore pressure values indicate regions of hydrostatic tension, i.e, tissue dilatation or expansion, and positive values represent regions of hydrostatic compression (tissue compression). All contour values are in MPa (N/mm^2). Note 0.001 MPa = 7.5 mmHg.

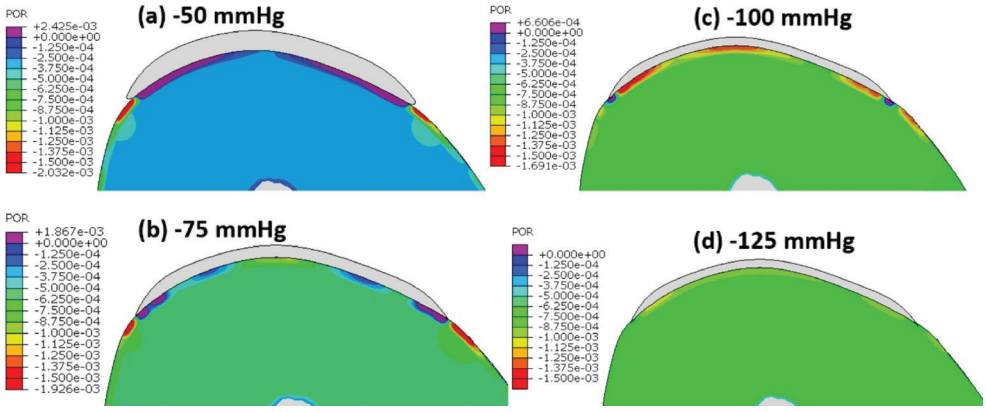

Figure 6 (A-D) Zoomed in view of dressing deformations (collapse) and interstitial fluid pressure contours as a function of increasing negative pressure (-50, -75, -100, -125 mmHg) at the 90-degree wrap angle. Negative pore pressure values indicate regions of hydrostatic tension, i.e., tissue dilatation or expansion, and positive values represent regions of hydrostatic compression (tissue compression). All contour values are in MPa (N/mm^2); Note 0.001 MPa = 7.5 mmHg.

poro-hyperelasticity (*SOILS, CONSOLIDATION*) module in ABAQUS™ (Dassault Systèmes Simulia Corp., 2017) to calculate the transient evolution of the coupled tissue deformation (strains) and interstitial fluid pressures (referenced in the model as "pore fluid pressures" or "pore-pressures") during the ramp loading and at the end of the 90-second hold time. Results were compared for the different scenarios, i.e., effects of the NP pressure level as well as the effects of the wrap angle.

RESULTS

Overall deformations

As the NP level is increased linearly from 0 to –125 mmHg (over 90 seconds) for the 90-degree dressing wrap angle, the dressing collapses within the negative pressure control volume created by the drape and the skin, with the skin and underlying tissue displacing upwards (Figure 5,6) and the drape/top surface of the foam deflecting

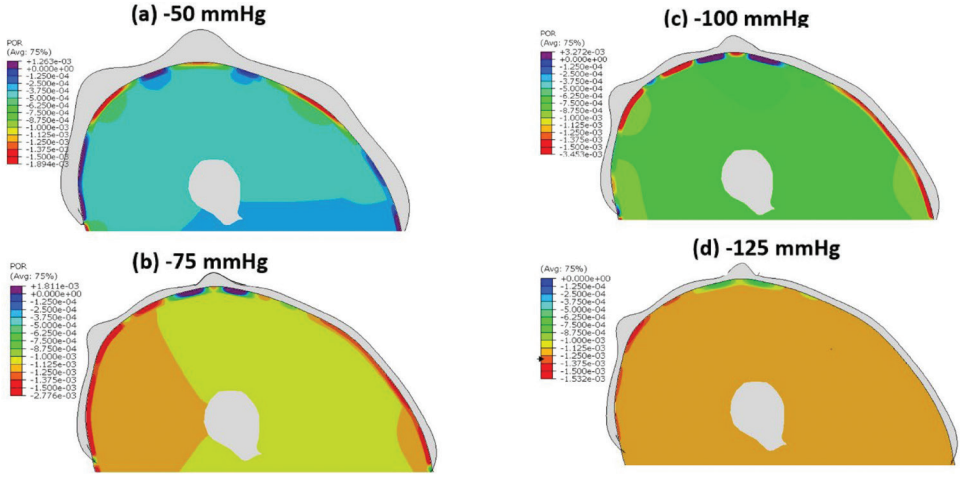

Figure 7(A-D) Zoomed in view of dressing deformations (collapse) and interstitial fluid pressure contours as a function of increasing NP (-50, -75, -100, -125 mmHg) at the 180-degree wrap angle. Negative pore pressure values indicate regions of hydrostatic tension, i.e., tissue dilatation or expansion, and positive values represent regions of hydrostatic compression (tissue compression). All contour values are in MPa (N/mm^2); Note 0.001 MPa = 7.5 mmHg.

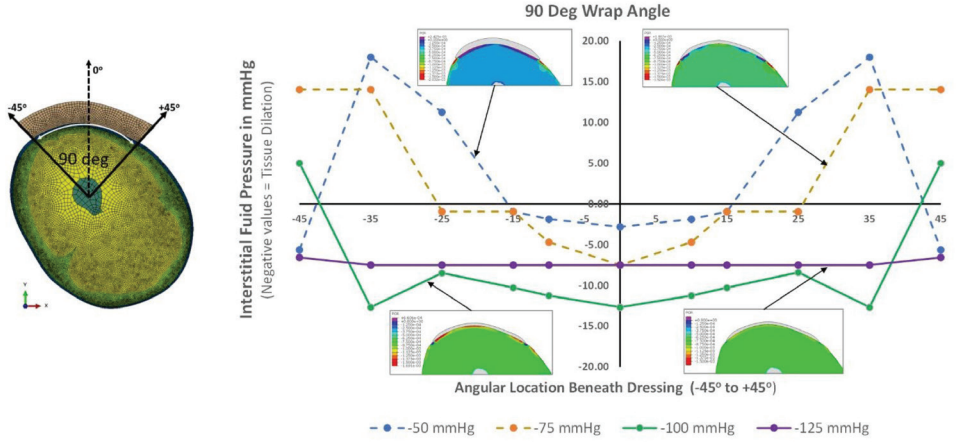

Figure 8 Angular distribution of interstitial fluid pressures in the region beneath the dressing contact for the 90-degree wrap angle cases. Note the dose response as a function of increasing levels of NP. At -50, and -75 mmHg, a substantial percentage of the arc of contact beneath the dressing experiences positive values (hydrostatic tissue compression). At higher levels of NP (-100 and –125 mmHg) the majority or the entirety of the tissue along the arc of contact experiences negative interstitial fluid pressures, i.e, **tissue dilatation/distention.**

downwards. This is typically seen in all applications of NPT. At higher wrap angles (180, 270, 360 degrees), "lobing" of the dressing is seen (Figures 7,10,12), a phenomenon which has been observed clinically as a higher order "wrinkling" of the foam dressing surface during application (Figure 11). In the current model, the mesh density (Figure 3) in this region of the dressing/foam is not refined enough to capture this high order wrinkling, as a result of which the observed deformation manifests as a coarser "lobing" morphology (Figures 7,10,12). However, mesh sensitivity studies indicated that this mesh size in this region of the model (i.e., the top surface of the dressing) does not affect the magnitude or distribution of NP at the dressing skin interface, or the resulting pore (interstitial) fluid pressures in the underlying tissue regions. Thus, the mesh density chosen was deemed to be sufficient to provide the desired simulation accuracy while balancing computational solution times (CPU time) and consistency of pore fluid pressure calculations in the simulations.

Pore (Interstitial) fluid pressures

In all the simulation results discussed in this study, negative values of interstitial fluid pressure represent tissue dilation/distension (hydrostatic tension) which is considered desirable from the perspective of achieving distension of lymphatic channels to enhance fluid ingress into the channels and achieve associated improvements in fluid clearance. Compressive (positive) values of interstitial fluid pressure represent tissue compression (hydrostatic) and are likely less desirable from the standpoint of engaging lymphatic channels. Results for interstitial fluid pressures were processed from the models to examine the region of tissue directly beneath the dressing contact and excluding the drape tension induced edge effects in the tissue regions adjacent to the contact zone.

90-Degree Wrap Angle Results: At the 90-degree wrap angle, a very interesting dose-response relationship is observed between applied NP and the resulting interstitial fluid pressures (Figure 8) with peak values of negative (tensile) interstitial (pore) fluid pressure seen at -100 mmHg. In addition, it is important to note the angular variation of interstitial fluid pressures along the arc of contact between dressing and tissue (Figure 8), and the associated extent (or percentage) of tissue engagement which also depicts a dose response dependency on NP. Notably, at lower NP levels (-50, -75 mmHg), significant portions of the tissue beneath the dressing experience high positive interstitial fluid pressures (compressive). With elevation in NP to –100 mmHg, peak values of negative fluid pressures are seen, in addition to which, most of the tissue (>90%) beneath the dressing experiences negative interstitial pressures, (Figure 8), indicating

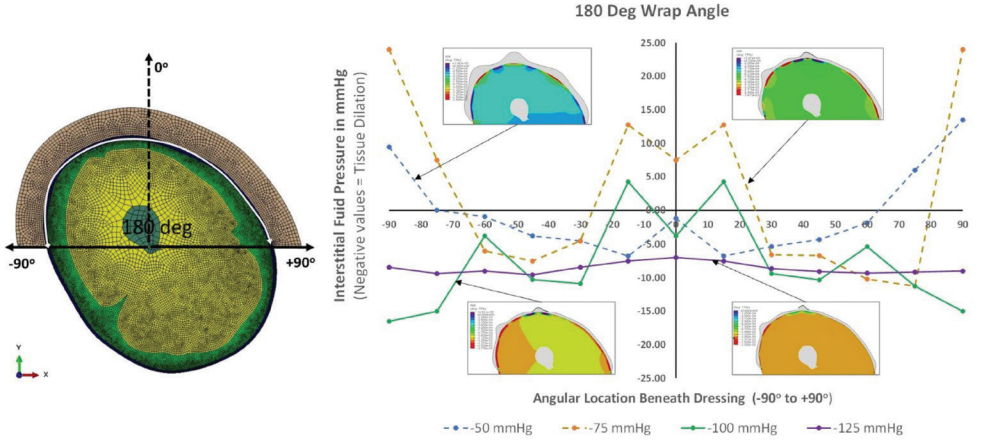

Figure 9 Angular distribution of interstitial fluid pressures in the region beneath the dressing contact for the 180-degree wrap angle cases. Note the dose response as a function of increasing levels of NP. At -50, and -75 mmHg, a substantial percentage of the arc of contact beneath the dressing experiences positive values (hydrostatic tissue compression). At higher levels of NPT (-100mmHg and -125mmHg) the majority or the entirety of the tissue along the arc of contact experiences negative interstitial fluid pressures, i.e., **tissue dilatation/distention.**

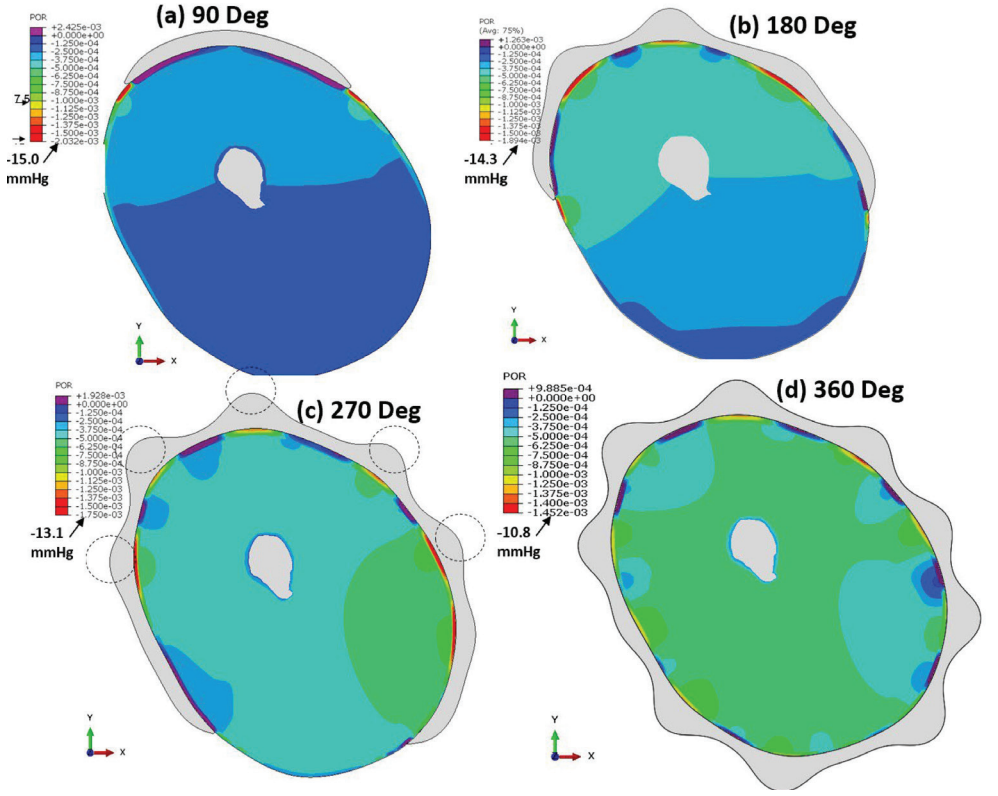

Figure 10 (A-D) Deformations and Interstitial fluid (pore) pressures at NP level of –50 mmHg across 4 different dressing wrap angles (90-360 degrees). Note the lobing of the drape/foam top surface at higher wrap angles (see Fig 7). Negative pore pressure values indicate regions of hydrostatic tension, i.e., tissue dilatation or expansion, and positive values represent regions of hydrostatic compression (tissue compression). All contour values are in Mpa (N/mm^2); Note 0.001 Mpa = 7.5 mmHg.

tissue distension/expansion. Finally at an NP level of -125 mmHg, while the peak interstitial pressure is lower than the value achieved at -100 mmHg, it is noted that the entirety (100%) of the tissue along the arc of contact with the dressing experiences negative interstitial fluid pressures.

180-degree wrap angle results: Very similar trends are observed at the 180-degree wrap angle (Figure 9), with substantial portions of tissue experiencing compressive (positive) values of interstitial fluid pressures at the lower NP levels (-50, -75 mmHg). The highest values of negative interstitial pressures (tissue distension) are again achieved at the

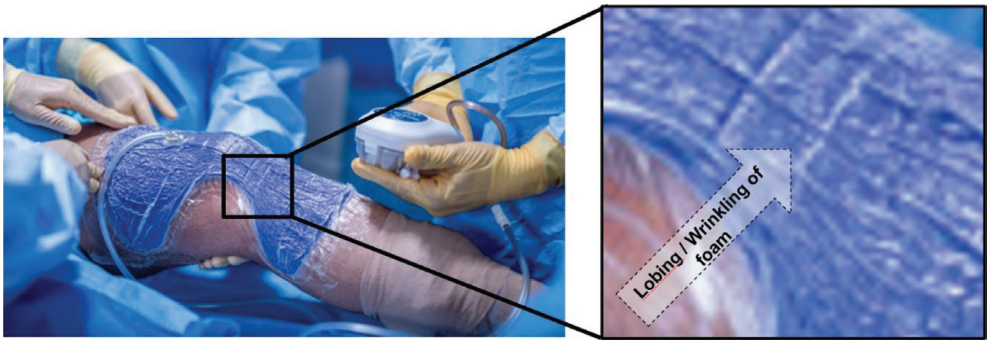

Figure 11 Close up of dressing deformations during NP application showing the lobing or wrinkling phenomenon seen as the foam collapses under NP. This validates the lobing mechanism observed in the FEA models (Figure 7)

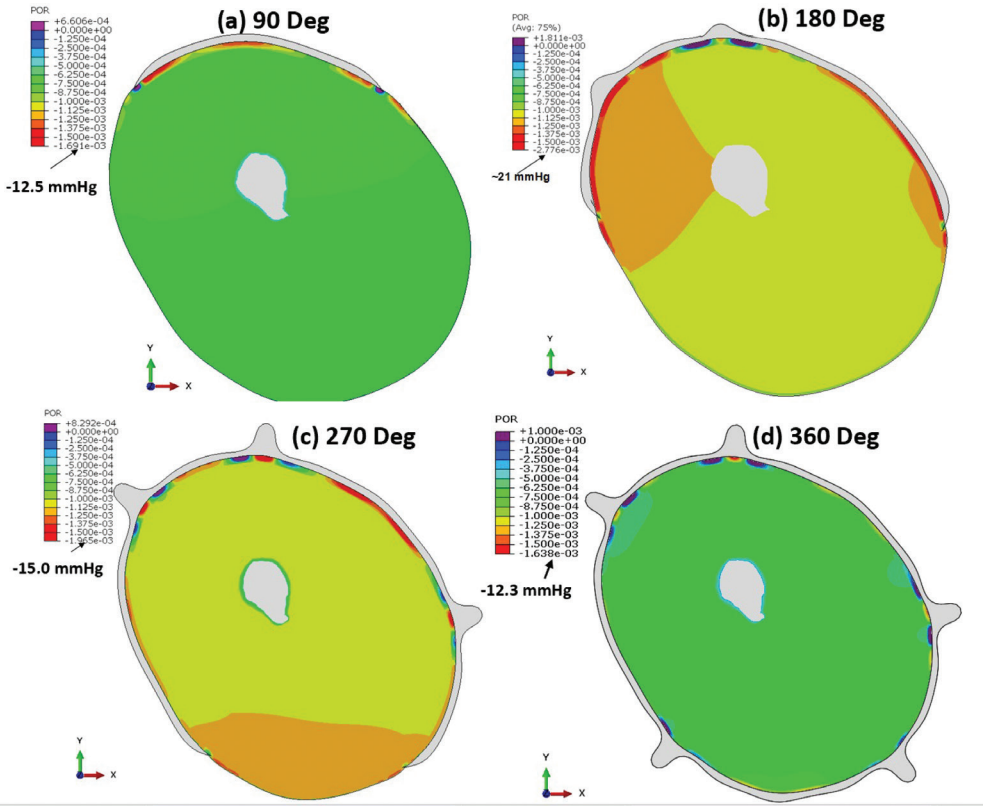

Figure 12 (A-D) Deformations and Interstitial fluid (pore) pressures at NP level of –100 mmHg across 4 different dressing wrap angles (90-360 degrees). Note the lobing of the drape/foam top surface at higher wrap angles (see Fig 7). Negative pore pressure values indicate regions of hydrostatic tension, i.e, tissue dilatation or expansion, and positive values represent regions of hydrostatic compression (tissue compression). All contour values are in Mpa (N/mm^2); Note 0.001 Mpa = 7.5 mmHg.

-100 mmHg level, albeit localized to small regions of the tissue along the arc of contact, with other regions experiencing positive values (Figure 9). As in the case of the 90-degree wrap angle, elevation of NP to -125mmHg for the 180-degree wrap condition achieves complete negative pressure engagement of the tissue along the entirety (100%) of the arc of contact beneath the dressing (Figure 9).

This dose-response with rising NP level is recapitulated at the other dressing wrap angles with the peak values of interstitial fluid pressures achieving a maximal value and then dropping at higher NP levels. Notably, at any level of NP, an increase in wrap angles from 90 to 360 degrees generally results in elevations in negative fluid pressures (Figures 10, 12). However, it is evident that wrap angle increases to 270 or even 360 degrees do not appear to significantly increase the magnitude or peak value of negative interstitial fluid pressures, although there is a greater volume of tissue engaged in distention (negative fluid pressure), which can be explained on the basis of the increased arc of contact. Concurrently, increased engagement of a larger volume of tissue beneath the dressing is observed all along the increased arc length of the dressing contact zone (Figure 10,12). Like the trends seen for the 90-degree wrap angle, higher wrap angles also produce compressive interstitial fluid (positive) pressures at the lower NP levels which change to hydrostatic tensile (negative) values as NP levels are increased (Figure 12). This is likely due to the evolving interface contact conditions between dressing and skin, and the time-dependent/transient effect of interstitial pressurization and fluid redistribution.

Overall trends in peak negative interstitial fluid pressures

Interstitial fluid pressures are examined in terms of the peak negative values achieved as a function of

NP level and wrap angle (Figure 13). In addition, the extent of tissue engagement along the arc of contact is also examined, expressed as the percentage of the tissue along length/arc of contact that experiences negative values of interstitial pressure (Figure 14).

At the 90- and 180-degree wrap angles, the highest values of interstitial negative fluid pressures are seen at -100 mmHg, with interstitial pressures dropping to lower levels at NP of -125 mmHg (Figure 13). However, while the peak values of interstitial pressures are lower at the -125 mmHg NP level, it is important to note that at this level of NP, 100% of the tissue beneath the arc of contact experiences negative interstitial fluid pressures (Figure 14). At NP levels of -50 mmHg and -75mmHg, only about 37-77% of the arc of contact experiences negative fluid pressures for the 90- and 180-degree wrap angle conditions.

In contrast, at the 270- and 360-degree wrap angles, the highest values of interstitial fluid pressures are observed at -75 mmHg (Figure 13), although it is evident that these peaks are highly localized to

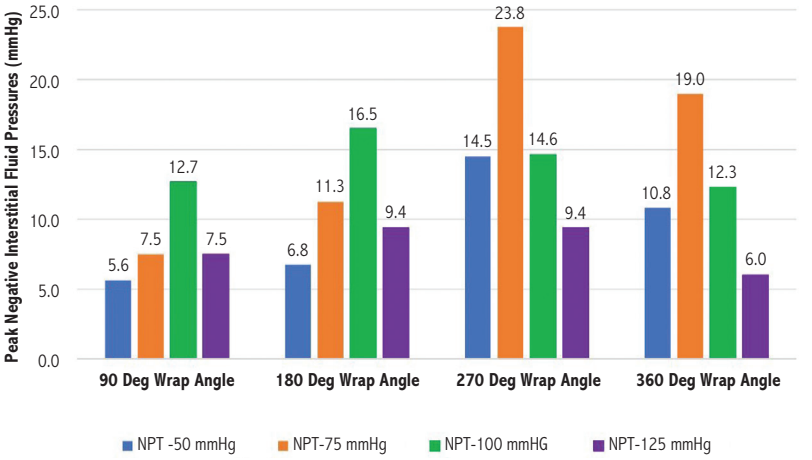

Figure 13 Dose response relationship between applied NP, wrap angle, and peak value of negative interstitial fluid pressures (hydrostatic tension values producing tissue expansion) beneath the dressing. *Notable, at lower angles, peak values are very localized in small zones of the dressing-tissue contact (Figure 6A, 6B; Figure 7A, 7B).* Also see Figure 14 that quantifies the length of tissue along the arc of contact that experiences negative interstitial fluid pressures)

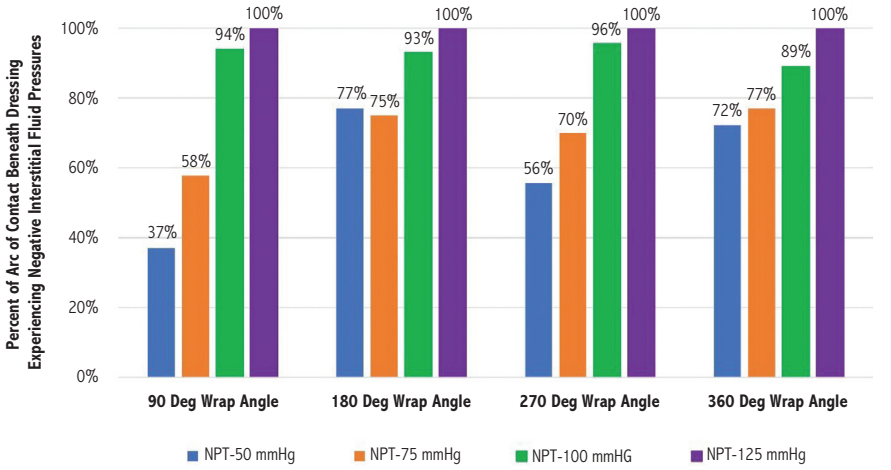

Figure 14 Dose response relationship between applied NP, wrap angle, and the percentage of the arc of contact beneath the dressing where tissue experiences negative interstitial fluid pressures (hydrostatic tension values) beneath the dressing that produces tissue expansion.

small regions of tissue beneath the dressing contact zone (Figure 10,12,14) with less than 75% of the arc of contact experiencing negative interstitial fluid pressures. Notably, at these wrap angles (270 and 360 degrees), elevation of NP levels to -100 mmHg and-125 mmHg results in 90-100% tissue engagement along the entire arc of contact and a negative interstitial pressure.

Overall, it appears that at the higher NP levels (> -100 mmHg) a substantial volume of tissue beneath the arc of contact experiences time varying interstitial fluid pressures that are negative (tensile), signifying a **predominant tissue dilation effect during application of NPT to intact skin**. The transient variations in interstitial pressures can be attributed to evolving dressing contact, NP level, diffusion/flow of tissue fluid, and most importantly regional heterogeneity as well as patient-to-patient variations in tissue mechanical and fluid permeability properties.

DISCUSSION

The poro-hyperelasticity simulations indicate that application of NPT to intact skin encompassing 90 to 360 degrees of a limb's circumference can trigger dispersed tissue expansion, rather than compression, immediately beneath the dressing, especially at NP levels exceeding –100 mmHg. The calculated negative interstitial fluid pressures imply tissue dilation or volumetric expansion in the 2-5 mm deep region immediately below the dressing-tissue interface. The magnitudes of negative fluid pressures beneath the dressing are approximately one order of magnitude lesser than the applied surface NP levels, and along with the depth of the effect (a few mm) provides some insight into the energy dissipation of NP into the underlying tissue layers. Most notably, negative interstitial fluid pressures imply tissue dilatation (volumetric expansion) which could open lymphatic pores, potentially allowing for fluid clearance. These results could partially explain the mechanism observed in porcine preclinical studies wherein NPT applied to closed incision sites produces statistically significant reductions in hematomas and seromas and increased lymphatic clearance concomitant with reduced fluid collection in the wound canister (Kilpadi & Cunningham, 2011). The presence of tissue dilation (or distension) and negative pore pressures of similar magnitudes has also been observed in similar computational models investigating the application of NPT to the intact skin of the forearm (Livarinen et al., 2016).

The study results show a strong dose dependent (NP level and wrap angle) effect on temporal peak values and spatial distribution of interstitial fluid pressures in the tissue beneath the dressing. The maximal effect, as measured by 2 parameters, peak negative interstitial pressures (Figure 13) and the percentage of tissue contact experiencing negative pressures (Figure 14) appears to be between -100 and -125 mmHg, with tissue engagement depths from 2 to 5 mm below the dressing contact interface. While there is a dose dependence on both NP level and wrap angle, it appears that the NP levels greater than –100 mmHg erase any effects of the wrap angle dependence especially when evaluated based on percentage tissue engagement underneath the dressing contact.

The occurrence of the peak at -100 mmHg (90- and180-degree wrap angles), and at -75 mmHg (270- and 360-degree wrap angles) in the current modeling work is a function of the tissue permeability coefficients and the elasticity of the solid phase which establish the time scale over which the fluid pressure equilibrates within the control volume (limb cross section). If permeability is lower than these values, the time scale to achieve equilibrium would be higher and peak values would be achieved at later times and higher NP levels. Similarly, variations in the solid phase tissue properties would also change the transient levels of interstitial fluid pressures and the associated maximal values achieved during the 90-second ramp phase of the NP application. For example, tissue properties (solid phase as well as permeability values) could vary in actual patients due to underlying chronic diseases such as venous insufficiency, diabetes, and peripheral artery disease.

This study also reveals the importance of examining the extent of tissue engagement via NPT, as measured in this work via the percentage of the arc of tissue contact length that experiences negative interstitial fluid pressures. While peak values of negative interstitial pressure provide some insight into dose response, the arc of contact is a powerful metric that enables a more balanced interpretation of the results via examination of the entire influence zone under the dressing contact region. Future preclinical studies, as well as clinical studies should be explored in conjunction with these computational

modeling and sensitivity studies to further quantify these effects and evolve our understanding of the MOA underlying the application of NPT to intact skin.

The MOA of NPT applied to intact skin or closed surgical incisions is likely very different from compression therapy and merits discussion and further research. The mechanics of interstitial fluid transport is based on the movement of fluid between 3 compartments, i.e., the arterial capillary bed, the tissue compartment interstitial space, and the initial lymphatics which serve as the entry point for interstitial fluid and the subsequent transport through the lymphatic capillaries to the draining lymph nodes. It is likely that NPT introduces a fundamentally different set of biomechanical interactions between these 3 compartments compared to compression therapies commonly used for clinical management of swelling and seroma incidence. While compression therapy works via interstitial fluid compression which controls fluid egress from the arterial capillary bed into the tissue and subsequently the lymphatics, NPT produces distension in the tissue layers inducing negative interstitial fluid pressures. Tissue distension induced by NPT is also likely to affect the biomechanical interaction between the collagen network in the interstitial compartment and the anchoring filaments connecting this network to the initial lymphatics (Arasa et al., 2021), posing the question whether NPT participates in enhancing fluid ingress into the lymphatics. NPT could also produce cyclical extrinsic biomechanical pressures around the lymphatic capillaries to further impact drainage. While the model currently does not have the ability to answer these questions, it does for the first time demonstrate the presence of tissue distension and subsequently the possible new mechanisms at play in terms of lymphatic clearance that is worth investigating in experimental and computational studies.

Study limitations

It is important to note some limitations of the current simulation-based study. By modeling a 2D planar cross section, these models assume that all the tissue deformation and interstitial fluid transport takes place within this section. In addition, the tissue is assumed to be a passive fluid-saturated solid volume with the implicit assumption that conservation of mass applies, i.e., the total volume of interstitial fluid available in the cross section is constant. This assumption implies that there is no source term (arterial capillary bed) that will or could introduce more fluid into the interstitial space. Similarly, there is also no sink term (lymphatics and venous) that remove fluid from the tissue. These assumptions imply that all fluid movement is redistribution of this fixed volume of fluid due to interstitial pressure gradients occurring in response to the NP applied over the time scale of the simulation in this model. Future models should consider 3D geometries to develop a better understanding of the out-of-plane fluid pressures, although such models will not necessarily address the more complex issue of source (capillary bed) and sink (lymphatic vessel) terms. Accurate modeling of the transport mechanisms will need more sophisticated approaches to capture the hierarchical structures at multiple length scales and the net result of the structure of the arterial capillary bed, tissue, and lymphatics on the movement of free fluid.

It is also noted that the model results are specific to a set of tissue material properties (solid phase hyperelastic constants, and fluid phase permeabilities), which are treated as *controlled variables* in this study, since the primary objective of this work was to examine the effect of NP level and dressing wrap angle (*independent variables*) on the interstitial fluid pressures (*response measure/ dependent variable*). Despite these limitations in the current work, it is important to note that these models provide important insight and quantify the extent of the interstitial fluid pressurization effect in tissue beneath the dressing contact zone, in response to NP loading on intact skin. At the same time this work highlights the need for future in vitro experiments and computational modeling in parallel with preclinical in vivo evaluations to establish the foundational principles of this important MOA of NPT on intact skin.

SIGNIFICANCE

Patient outcomes after major surgeries like total knee arthroplasty (TKA) are impacted during the post operative management phase which in the current clinical setting involves coordination between surgical drains, swelling management, and infection prevention. With the most important goals being restoration of normal range of motion and recovery during physiotherapy and rehabilitation, it is exceedingly important to develop new strategies

to reliably manage complications like seroma and swelling. NPT provides a new alternative to the clinician in terms of the ability to more precisely tailor post-operative treatment protocols using NPT, such as NP level, dressing wrap angle, and the application of cyclic or continuous NP. The likely effect of NPT in terms of actuating the lymphatic pores (initial lymphatics) as well as lymphatic capillaries to enhance fluid clearance without drain collection is potentially attractive to the personnel involved in post operative management (surgeons and nurses), and most importantly the patients who may be able to navigate challenging physiotherapy with lesser pain. Application of NPT could reduce post-operative edema around the incision site and surrounding tissue envelope, for example following a TKA surgical procedure. Reducing edema following a surgical procedure such as a TKA may help facilitate early ambulation and patient compliance with post-operative rehabilitation protocols, potentially helping with muscle strength restoration and range of motion, thereby helping improve the prognosis for improved long-term recovery.

ACKNOWLEDGMENT

We thank the following Solventum (formerly 3M Company) employees, Marisa Schmidt, Manny Landez, Mason Haggerty and Kurt Hudson, for providing input and perspective based upon their experiences in the field and for their careful reviews of the manuscript. Samantha Mann and Animesh Agarwal, M.D. are gratefully acknowledged for creating the graphics and providing the clinical images, respectively, used in Figure 1.

FUNDING

This study was funded by Solventum (Formerly 3M Company).

NOMENCLATURE

NPT	Negative Pressure Therapy
ciNPT	Closed Incision Negative Pressure Therapy
NP	Negative Pressure
TKA	Total knee arthroplasty
FEA	Finite element analysis
MOA	Mechanisms of Action

REFERENCES

Arasa, J., Collado-Diaz, V., & Halin, C. (2021). Structure and immune function of afferent lymphatics and their mechanistic contribution to dendritic cell and T cell trafficking. *Cells, 10*(5), 1269. https://doi.org/10.3390/cells10051269

Barsimantov, J., Payne, J., de Lucio, M. *et al*. Poroelastic Characterization and Modeling of Subcutaneous Tissue Under Confined Compression. *Ann Biomed Eng* **52**, 1638–1652 (2024). https://doi.org/10.1007/s10439-024-03477-1

Brock, T. M., Sprowson, A. P., Muller, S., & Reed, M. R. (2017). Sticks study – short-stretch inelastic compression bandage in knee swelling following total knee arthroplasty – a feasibility study. *Trials*, *18*(1). https://doi.org/10.1186/s13063-016-1767-5

Dassault Systèmes Simulia Corp. (2017). *ABAQUS™ software* [Computer software]. Johnston, RI, USA.

Fahlgren, A., Johansson, L., Edlund, U., & Aspenberg, P. (2012). Direct ex vivo measurement of the fluid permeability of loose scar tissue. *Acta Bioengineering and Biomechanics, 14*(2), 47–51. https://pubmed.ncbi.nlm.nih.gov/22793501

Hendriks, F.M., & Hendriks, F.M. (2005). *Mechanical behaviour of human epidermal and dermal layers in vivo*. Technische Universiteit Eindhoven.

Holm, B., Kristensen, M. T., Bencke, J., Husted, H., Kehlet, H., & Bandholm, T. (2010). Loss of knee-extension strength is related to knee swelling after total knee arthroplasty. *Archives of Physical Medicine and Rehabilitation*, *91*(11), 1770–1776. https://doi.org/10.1016/j.apmr.2010.07.229

Kilpadi, D. V., & Cunningham, M. R. (2011). Evaluation of closed incision management with negative pressure wound therapy (cim): Hematoma/Seroma and involvement of the lymphatic system. *Wound Repair and Regeneration*, *19*(5), 588–596. https://doi.org/10.1111/j.1524-475x.2011.00714.x

Lavigne T, Urcun S, Fromy B, Josset-Lamaugarny A, Lagache A, Suarez-Afanador CA, Bordas SPA, Rohan PY, Sciumè G. Hierarchical Poromechanical Approach to Investigate the Impact of Mechanical Loading on Human Skin Micro-Circulation. Int J Numer Method Biomed

Eng. 2025 Jul;41(7):e70066. https://doi: 10.1002/cnm.70066. PMID: 40650462; PMCID: PMC12254909.

Livarinen, J. T., Korhonen, R. K., & Jurvelin, J. S. (2016). Modeling of interstitial fluid movement in soft tissue under negative pressure – relevance to treatment of tissue swelling. *Computer Methods in Biomechanics and Biomedical Engineering,19*(10),1089–1098. https://doi.org/10.1080/10255842.2015.1101073

Munk, S., Jensen, N. J., Andersen, I., Kehlet, H., & Hansen, T. B. (2013). Effect of compression therapy on knee swelling and pain after total knee arthroplasty. *Knee surgery, sports traumatology, arthroscopy: official journal of the ESSKA*, *21*(2), 388–392. https://doi.org/10.1007/s00167-012-1963-0

Oomens, C. W. J., Bressers, O. F. J. T., Bosboom, E. M. H., & Bouten, C. V. C. (2001). Deformation analysis of a supported buttock contact. In R. D. Kamm (Ed.), *Proceedings of the 2001 Bioengineering conference: Snowbird, Utah, June 27-July 1, 2001* (pp. 853-854). (BED; Vol. 50). American Society of Mechanical Engineers.

Oomens, C. W. J., van Campen, D. H., & Grootenboer, H. J. (1987). A mixture approach to the mechanics of skin. *Journal of Biomechanics*, *20*(9), 877–885. https://doi.org/10.1016/0021-9290(87)90147-3

Pachowsky, M., Gusinde, J., Klein, A., Lehrl, S., Schulz-Drost, S., Schlechtweg, P., Pauser, J., Gelse, K., & Brem, M. H. (2012). Negative pressure wound therapy to prevent seromas and treat surgical incisions after total hip arthroplasty. *International orthopaedics*, *36*(4), 719–722. https://doi.org/10.1007/s00264-011-1321-8

Pauser, J., Nordmeyer, M., Biber, R., Jantsch, J., Kopschina, C., Bail, H. J., & Brem, M. H. (2014). Incisional negative pressure wound therapy after hemiarthroplasty for femoral neck fractures – reduction of wound complications. *International Wound Journal*, *13*(5), 663–667. https://doi.org/10.1111/iwj.12344

Stannard, J. P., Atkins, B. Z., O'Malley, D., Singh, H., Bernstein, B., Fahey, M., Masden, D., & Attinger, C. E. (2009). Use of negative pressure therapy on closed surgical incisions: a case series. *Ostomy/wound management*, *55*(8), 58–66.

Stannard, J. P., Robinson, J. T., Anderson, E. R., McGwin, G., Volgas, D. A., & Alonso, J. E. (2006). Negative pressure wound therapy to treat hematomas and surgical incisions following high-energy trauma. *The Journal of Trauma: Injury, Infection, and Critical Care*, *60*(6), 1301–1306. https://doi.org/10.1097/01.ta.0000195996.73186.2e

Stannard, J. P., Volgas, D. A., Stewart, R., McGwin, G., & Alonso, J. E. (2009). Negative pressure wound therapy after severe open fractures: A prospective randomized study. *Journal of Orthopaedic Trauma*, *23*(8), 552–557. https://doi.org/10.1097/bot.0b013e3181a2e2b6

Szöts, K., Pedersen, P. U., Hørdam, B., Thomsen, T., & Konradsen, H. (2015). Physical health problems experienced in the early postoperative recovery period following total knee replacement. *International Journal of Orthopaedic and Trauma Nursing*, *19*(1), 36–44. https://doi.org/10.1016/j.ijotn.2014.03.005

Xu, W., Zheng, Y., Yin, Z., Jiang, Y., Zhang, Z., Ma, S., Cao, Y., Imaging the intramuscular pressure of living muscles with shear waves, *Journal of the Mechanics and Physics of Solids,*Volume 192, 2024, 105834, ISSN 0022-5096, https://doi.org/10.1016/j.jmps.2024.105834.

Wheatley, B. B., Odegard, G. M., Kaufman, K. R., & Haut Donahue, T. L. (2017). A case for poroelasticity in skeletal muscle finite element analysis: Experiment and modeling. *Computer Methods in Biomechanics and Biomedical Engineering, 20*(6), 598–601. https://doi.org/10.1080/10255842.2016.1268132

Wilkes, R. P., et al. (2012). Closed incision management with negative pressure wound therapy (CIM): Biomechanics. *Surgical Innovation, 19*(1), 67–75. https://doi.org/10.1177/1553350611414920